Eur. Phys. J. B **46**, 331–334 (2005)
DOI: 10.1140/epjb/e2005-00262-8

THE EUROPEAN PHYSICAL JOURNAL B

Quantum interference in carbon nanotube intramolecular junction

F. Hu[a], W. Fa, and J. Dong

Group of Computational Condensed Matter Physics, National Laboratory of Solid State Microstructures, and Department of Physics, Nanjing University, Nanjing, 210093, P.R. China

Received 8 January 2005 / Received in final form 29 May 2005
Published online 18 August 2005 – © EDP Sciences, Società Italiana di Fisica, Springer-Verlag 2005

Abstract. The quantum conductance oscillations (QCOs) of the intramolecular junction (IMJ) composed of two single-wall carbon nanotubes (SWNTs) have been studied by using a π-orbital only tight-binding (TB) model and a Green's function technique. It is found that in the IMJs in addition to the rapid QCO frequencies corresponding to the constituent tubes there exist also their sum frequencies. The slow QCO frequencies of the IMJ will be different from those of its corresponding two perfect tubes if they have different chiral angles.

PACS. 73.40.Jn Metal-to-metal contacts – 73.63.Fg Nanotubes – 73.22.-f Electronic structure of nanoscale materials: clusters, nanoparticles, nanotubes, and nanocrystals

1 Introduction

As electronic devices shrink to be comparable to their electron coherence length, the quantum interference between electron waves in the devices becomes important, and this leads to dramatic changes in the devices properties [1–8]. An example of the coherent electronic device is the Fabry-Perot electron resonator based on individual SWNT with near-perfect ohmic contacts to electrodes, in which the rapid and slow quantum conductance oscillations (QCOs) have been observed [9,10]. Jiang et al. have shown that both the rapid and slow QCOs are ascribed to the intrinsic quantum interference. They also demonstrate that the rapid QCO depends only on the tube length, while the slow one depends on not only the tube length, but also its chirality [11]. These conclusions have been verified by the numerical simulations [12].

A SWNT can be a metal or a semiconductor, depending on its helicity and diameter [13–16]. Two SWNTs with different helicities and diameters can form a metal-semiconductor (M-S), metal-metal (M-M) or semiconductor-semiconductor (S-S) IMJ by introducing the pentagon-heptagon defects, which could be the building blocks of the nano-electronic and electro-optical devices. The electronic properties of the IMJs have been widely theoretically considered [17–21], such as Tamura et al. have been studied the reflection and transmission of electron waves at many M-M IMJs [22]. And recently, Ouyang et al. have found experimentally the SWNT IMJs [23].

[a] e-mail: hu010@sina.com.cn

Although the quantum interference in the perfect SWNT and the electronic properties of IMJs have been widely investigated, the quantum interference of the IMJs has not yet been studied until now, making related problems unclear. For example, it is not known whether or not the sum frequency of the constituent tubes exists, and what is the effect of the junction on the rapid and slow QCOs. In this paper, we will numerically calculate the quantum interference of two M-M IMJs by using the TB-based Green's-function approach [24]. Our results show that exists the sum frequency of the oscillation frequencies corresponding to those of the constituent tubes, and the junction has little influence on the rapid QCO frequency in our models.

The paper is organized as follows: in Section 2, we introduce the models and calculation method. In Section 3, the results and discussions are given. The concluding remarks are made in Section 4.

2 Models and method

The whole model system consists of the central sample (the SWNT IMJ) and two semi-infinite leads (left and right), which, for simplicity, are taken to be the same tubes as those forming the IMJ. For comparison, we have constructed two types of M-M IMJs, i.e., the (12, 0)-(6, 6) and (8, 2)-(6, 6), formed along a common axis, which are produced by introducing two and four pairs of pentagon-heptagon (5-7) defects, respectively. The final geometrical structures of the IMJs are illustrated in Figure 1.

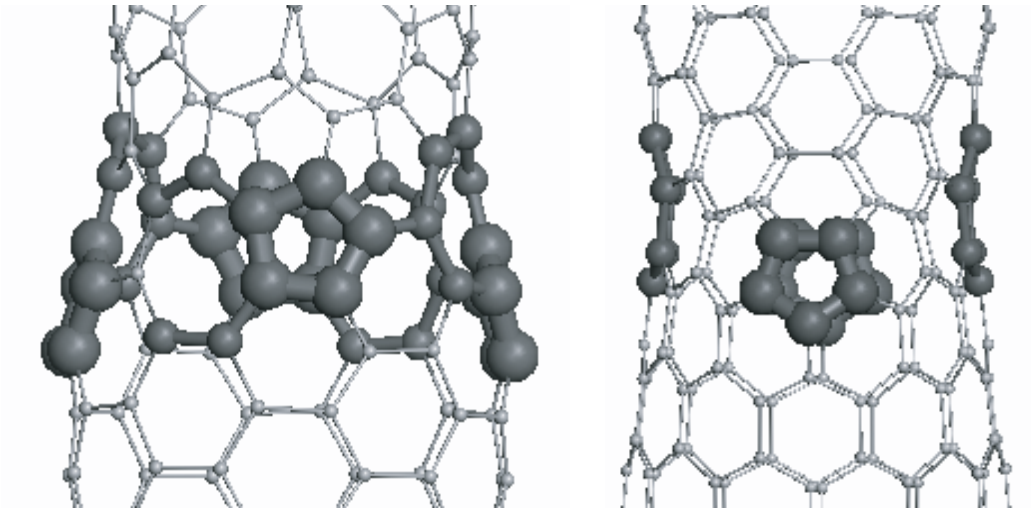

(a) (b)

Fig. 1. The geometrical structures of (a) (8, 2)-(6, 6) IMJ and (b) (12, 0)-(6, 6) IMJ. The defect atoms are represented by black balls. The big (small) balls represent pentagons (heptagons).

In the following, we will use the symbol of $(m,n)k$ to represent the (m,n) SWNT with k unit cells. In our models the constituent tubes forming the IMJs are (12, 0) 40 (168.739 Å), (6, 6) 164 (401.563 Å), and (8, 2) 29 (187.984 Å), respectively.

The IMJ can be described in the TB approximation with one π-orbital per atom. The Hamiltonian of the central IMJ can be written as

$$H_c = V_{pp\pi} \sum_{\langle i,j \rangle} a_i^\dagger a_j + H.c.,$$

where the sum over i, j is restricted to the nearest-neighbor atoms, and the on-site energies have been set to zero. In our calculations all the nearest-neighbor hopping parameters are assumed to be $V_{pp\pi} = -2.75$ eV [17], except those nearby the lead contacts, where they are taken to be $\alpha V_{pp\pi}$ with $0 < \alpha < 1$, making electrons slightly scattered at the interfaces. In our calculations, $\alpha = 0.8$ has been taken [25]. The system conductance G can be calculated by the Landauer formula $G = \left(2e^2/h\right) T$, with T the transmission coefficient, which is expressed as follows [2,26,27]

$$T = \mathrm{Tr}\left(\Gamma_L G_C^r \Gamma_R G_C^a\right).$$

Here, G_C^r, G_C^a are the retarded and advanced Green's functions of the IMJ, respectively, and $\Gamma_L\left(\Gamma_R\right)$ is the coupling matrix of the IMJ to the left (right) lead.

The Green's function $G_C\left(E\right)$ of the IMJ can be written as

$$G_C\left(E\right) = \left(E - H_C - \Sigma_R - \Sigma_L\right)^{-1},$$

and the coupling matrix $\Gamma_L\left(\Gamma_R\right)$ is written as

$$\Gamma_{L(R)} = i[\Sigma_{L(R)}^r - \Sigma_{L(R)}^a].$$

Here, $\Sigma_L = h_{LC}^\dagger g_L h_{LC}$ and $\Sigma_R = h_{CR} g_R h_{CR}^\dagger$ are the self energy terms. h_{LC} and h_{CR} are the coupling matrices, which are nonzero for the adjacent points between the IMJ and the leads. $g_{L(R)} = \left(E - H_{L(R)}\right)^{-1}$ is the Green's functions of the left (right) lead.

3 Results and discussions

We have calculated the conductance vs. Fermi energy for two different IMJs, namely, (12, 0)-(6, 6) and (8, 2)-(6, 6), and their corresponding perfect tubes at zero temperature. The obtained results are shown in Figure 2.

Firstly, let us see the results of the perfect tubes in Figures 2a, 2b and 2c, all of which display remarkable rapid QCO superimposed on a slow fluctuation background except the zigzag (12, 0) 40 tube, and their maximum conductance approaches to $2G_0$. That is because the rapid and slow QCOs come from the linear and nonlinear terms of the energy dispersion relations, respectively, and for the zigzag tube, its dispersion relations of the two propagating modes are the same, leading to no the contribution from the nonlinear term [11]. The calculated rapid QCO frequencies for the perfect (6, 6) 164, (12, 0) 40 and (8, 2) 29 tubes are 21.912 $(\mathrm{eV})^{-1}$, 9.391 $(\mathrm{eV})^{-1}$ and 10.434 $(\mathrm{eV})^{-1}$, respectively. According to the analytical prediction,

$$\frac{1}{\Delta E_f} = \frac{2L}{3\pi V_{pp\pi} a_{c-c}} \approx \frac{L}{18.376}\ (\mathrm{eV})^{-1}$$

(a_{c-c} is the bond length and L the tube length in unit of Å), so, the QCO frequencies of these three tubes should be 21.853 $(\mathrm{eV})^{-1}$, 9.183 $(\mathrm{eV})^{-1}$, and 10.230 $(\mathrm{eV})^{-1}$, respectively. It is clearly seen that our calculated results agree very well with the analytical ones, among which, the biggest difference between the numerical and the analytical results is that of (12, 0) 40 tube, with its relative error of only 2.215%.

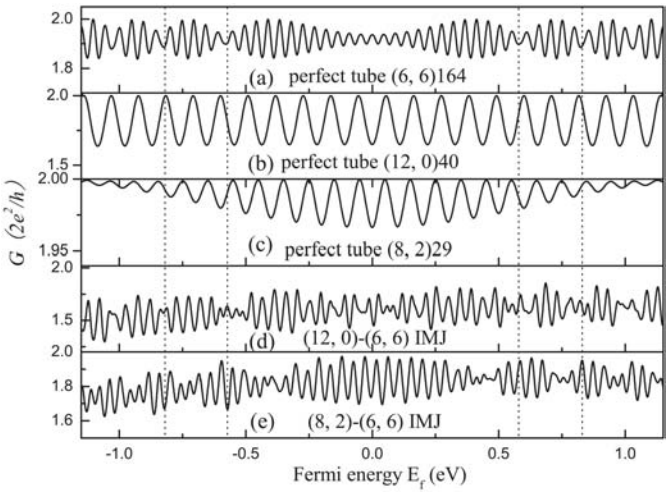

Fig. 2. Conductance G vs. Fermi energy E_f with $\alpha = 0.8$ for the three perfect tubes (a) (6, 6) 164, (b) (12, 0) 40, (c) (8, 2) 29, and their corresponding IMJs (d) (12, 0)-(6, 6), (e) (8, 2)-(6, 6). The four dot lines are used to make clear the difference of the slow QCOs between the IMJs and the perfect (6, 6) tube.

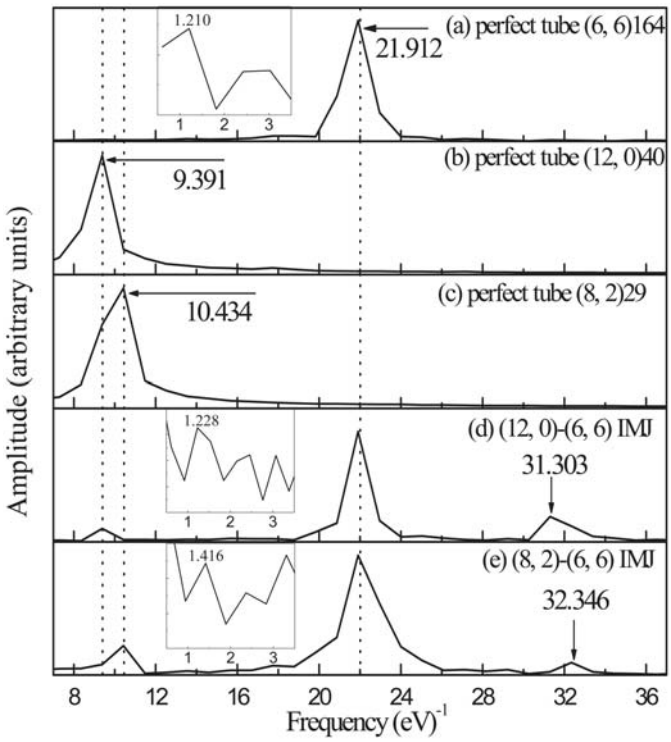

Fig. 3. The frequency analyses of the conductance oscillations for perfect tubes (a) (6, 6) 164, (b) (12, 0) 40, (c) (8, 2) 29, and their corresponding IMJs (d) (12, 0)-(6, 6), (e) (8, 2)-(6, 6). The dot lines denote the positions of the rapid QCO frequencies of the perfect tubes. The numerical values in (d) and (e) labeled by the vertical arrows are the sum frequencies of the QCOs in the IMJs. The slow QCO frequencies are shown in the insets.

Then, let us look at the results for the (12, 0)-(6, 6) and (8, 2)-(6, 6) IMJs, shown in Figures 2d and 2e. As expected, the maximum conductance of the IMJs becomes smaller than $2G_0$ because any defects will reduce the conductance, and in a combined A-B system, the subsystem B can be considered as a perturbation to the subsystem A, and vice versa. The rapid QCOs still exist in the both IMJs, though they show more irregular behavior. It is seen from Figure 2 that the perfect tube has only one rapid QCO frequency, but the IMJ has more rapid QCO frequencies. In order to see it clearly, we have done the corresponding frequency analyses of the QCOs, and shown the results in Figure 3, which indicate that the rapid QCO frequencies of the constituent tubes still can be found in their IMJ, and are almost not changed, demonstrating the junctions do not affect the rapid QCOs.

More importantly, It is clearly seen from Figures 3d and 3e that there exist new frequencies of 31.303 $(\text{eV})^{-1}$ and 32.346 $(\text{eV})^{-1}$, respectively for the (12, 0)-(6, 6) and (8, 2)-(6, 6) IMJs. The former is the sum of the rapid QCO frequencies, 9.391 and 21.912 $(\text{eV})^{-1}$, respectively for the perfect (12, 0) 40 and perfect (6, 6) 164 tubes. The latter is the sum frequency of those QCOs corresponding to the perfect tubes forming the (8, 2)-(6, 6) IMJ. On the other hand, the sum frequency can also be considered as a rapid QCO frequency corresponding to the whole IMJ length because the rapid QCO frequency only depends on the system length.

Finally, we discuss the slow QCOs of the IMJs in Figures 2d and 2e, from which we can see that the slow QCOs still appear in both IMJs, although they are more obviously seen in (8, 2)-(6, 6) IMJ than in (12, 0)-(6, 6) IMJ. Comparing Figures 2a, 2b and 2d, we can find the slow QCOs in (12, 0)-(6, 6) IMJ come only from the (6, 6) 164 tube, and its periods are very similar to that of the (6, 6) 164 tube, as denoted by the dot lines in the figure. From the insets in Figures 3a and 3d, the corresponding low-frequency analyses, can see clearly this conclusion, where the slow QCO frequency of (6, 6) 164 tube is about 1.210 $(\text{eV})^{-1}$ and that of the IMJ is about 1.228 $(\text{eV})^{-1}$. This result can be explained as follows. The slow oscillations come from the intrinsic quantum interference, and its periods depend on the length and chiral angle of the tube. When two SWNTs are connected along a common axis, their chiral angles and lengths change little, making so their slow QCO periods almost not changed. In addition, there is no slow conductance fluctuation in (12, 0) 40 tube, making the slow QCO of the (12, 0)-(6, 6) IMJ determined only by its constituent (6, 6) tube. On the other hand, for the (8, 2)-(6, 6) IMJ, both of its constituent tubes, (6, 6) and (8, 2) tubes, can have their own slow QCOs, and so the slow QCO of the (8, 2)-(6, 6) IMJ will be determined by both (6, 6) and (8, 2) tubes. It is seen from comparison between Figure 2a, 2c and 2e that the slow oscillations of the (8, 2)-(6, 6) IMJ are more similar to those of the (6, 6) tube except that in the central energy region near zero, which is more similar to the 1st slow QCO of the (8, 2) tube. It can be seen that indeed the 1st slow oscillation period of the IMJ is smaller than that of (6, 6) 164 tube. From insets of Figure 3e and 3a, it is known that the 1st slow frequencies of the (8, 2)-(6, 6) IMJ and the (6, 6) 164 tube are 1.416 $(\text{eV})^{-1}$ and 1.210 $(\text{eV})^{-1}$, respectively.

And from the analytical formula, we know the 1st slow frequency of the (8, 2) 29 tube is 0.219 $(\text{eV})^{-1}$. So, most probably, the 1st slow QCO of the (8, 2)-(6, 6) IMJ is the sum of the 1st QCOs of the (8, 2) and (6, 6) tubes.

4 Conclusion

In summary, we have studied the quantum interference of the metallic SWNT IMJs by using the TB Green's function technique. It is found that an IMJ, not only keeps the rapid QCO frequencies of its constituent tubes, but also can induce their sum frequency. The slow QCOs of the IMJ are also determined by the superposition of those of its constituent tubes.

This work was supported by the Natural Science Foundation of China under Grants Nos. A040108, 90103038, and 10474035.

References

1. T. Ando et al., *Mesoscopic Physics and Electronics* (Springer-Verlag, Berlin, 1998)
2. S. Datta, *Electronic Transport in Mesoscopic Systems* (Cambridge University Press, Cambridge, England, 1995)
3. B.J. van Wees, L.P. Kouwenhoven, C.J.P.M. Harmans, J.G. Williamson, C.E. Timmering, M.E.I. Broekaart, C.T. Foxon, J.J. Harris, Phys. Rev. Lett. **62**, 2523 (1989)
4. M.F. Crommie, C.P. Lutz, D.M. Eigler, Science **262**, 218 (1993)
5. Y. Ji, M. Heiblum, D. Sprinzak, D. Mahalu, H. Shtrikman, Science **290**, 779 (2000)
6. M.A. Topinka, B.J. LeRoy, S.E.J. Shaw, E.J. Heller, R.M. Westervelt, K.D. Maranowski, A.C. Gossard, Science **289**, 2323 (2000)
7. H.C. Manoharan, C.P. Lutz, D.M. Eigler, Nature **403**, 512 (2000)
8. P. Debray, O.E. Raichev, P. Vasilopoulos, M. Rahman, R. Perrin, W.C. Mitchell, Phys. Rev. B **61**, 10 950 (2000)
9. W. Liang, M. Bockrath, D. Bozovic, J.H. Hafner, M. Tinkham, H. Park, Nature **411**, 665 (2001)
10. J. Kong, E. Yenilmez, T.W. Tombler, W. Kim, H. Dai, Phys. Rev. Lett. **87**, 106801 (2001)
11. J. Jiang, J. Dong, D.Y. Xing, Phys. Rev. Lett. **91**, 056802 (2003)
12. L.F. Yang, J.W. Chen, H.T. Yang, J.M. Dong, Phys. Rev. B **69**, 153407 (2004)
13. J.W. Mintmire, B.I. Dunlap, C.T. White, Phys. Rev. Lett. **68**, 631 (1992)
14. N. Hamada, S.I. Sawada, A. Oshiyama, Phys. Rev. Lett. **68**, 1579 (1992)
15. R. Saito, M. Fujita, G. Dresselhaus, M.S. Dresselhaus, Appl. Phys. Lett. **60**, 2204 (1992)
16. T.W. Odom, J.L. Huang, P. Kim, C.M. Lieber, Nature **391**, 62 (1998)
17. L. Chico, V.H. Crespi, L.X. Benedict, S.G. Louie, M.L. Cohen, Phys. Rev. Lett. **76**, 971 (1996)
18. L. Chico, L.X. Benedict, S.G. Louie, M.L. Cohen, Phys. Rev. B **54**, 2600 (1996)
19. J.C. Charlier, T.W. Ebbesen, Ph. Lambin, Phys. Rev. B **53**, 11108 (1996)
20. W. Fa, J. Chen, H. Liu, J. Dong, Phys. Rev. B **69**, 235413 (2004)
21. R. Tamura, M. Tsukada, Phys. Rev. B **55**, 4991 (1997); R. Tamura, M. Tsukada, Phys. Rev. B **58**, 8120 (1998); R. Tamura, M. Tsukada, Phys. Rev. B **61**, 8548 (2000)
22. R. Tamura, M. Tsukada, Solid State Commun. **101**, 601 (1997)
23. M. Ouyang, J.-L. Huang, C.L. Cheung, C.M. Lieber, Science **291**, 97 (2001)
24. M.B. Nardelli, Phys. Rev. B **60**, 7828 (1999)
25. According to reference [12], when the contact coupling is strong, namely, the parameter α being large, the model system behaves as electron resonator, but when the contact coupling is very weak (the parameter α being small), the model system behaves like a quantum dot. Because we consider the behavior of electron resonator, we should choose a larger α. We have tested the effect of the parameter α value on the conductance oscillations, and have chosen $\alpha = 0.8$ in our calculation
26. D.S. Fisher, P.A. Lee, Phys. Rev. B **23**, 6851 (1981)
27. Y. Meir, N.S. Wingreen, Phys. Rev. Lett. **68**, 2512 (1992)